2015-07-01

Cellular Discrimination Using In Vitro Raman Micro Spectroscopy: The Role Of The Nucleolus

Hugh Byrne
Technological University Dublin, hugh.byrne@tudublin.ie

Recommended Citation

"Cellular discrimination using in vitro Raman micro spectroscopy: the role of the nucleolus", Z. Farhane, F. Bonnier, A. Casey, A. Maguire, L. O'Neill and H.J. Byrne, *Analyst*, 140, 5908-5919 (2015) doi:10.1039/c5an01157d

Funder: SFI

Analyst

PAPER

View Article Online
View Journal | View Issue

Cite this: *Analyst*, 2015, **140**, 5908

Cellular discrimination using *in vitro* Raman micro spectroscopy: the role of the nucleolus†

Z. Farhane,*[a] F. Bonnier,[b] A. Casey,[a] A. Maguire,[a] L. O'Neill[a] and H. J. Byrne[a]

Raman micro spectroscopy has attracted considerable attention over the last few years to explore its possible clinical applications as a non-invasive powerful label-free *in vitro* screening tool in cancer diagnosis and monitoring, subcellular analysis of biochemical processes, drug uptake, mode of action and mechanisms of interaction as well as toxicity of, for example, chemotherapeutic agents. However, in order to evaluate accurately the potential of Raman micro spectroscopy for such applications it is essential to optimise measurement and data processing protocols associated with subcellular analysis. To this end, *in vitro* differentiation of cell lines is a basic proof of concept for the potential of the technique, and although many studies have indicated successful differentiation based on Raman micro spectroscopy, it is important, as the measurement and processing techniques are improved, to establish the biochemical and subcellular basis of that discrimination. In this study, Raman micro spectroscopy is used to compare and differentiate normal and cancer cells from human lung origin, A549 adenocarcinoma cell line, Calu-1 epidermoid non-small-cell and BEAS-2B normal immortalized bronchial epithelium cell line. Spectra were taken from the three subcellular compartments, cytoplasm, nucleus and nucleolus and Principal Components Analysis was used to compare the spectral profiles between the cell lines and, coupled to Linear Discriminant Analysis, to explore the optimum sensitivity and specificity of discrimination. To support the analysis, Raman micro spectroscopy was coupled with Flow Cytometry, Confocal Laser Scanning Microscopy and Atomic Force Microscopy. While all subcellular regions can be employed to differentiate the normal and cancer cell lines, optimum discrimination sensitivity and specificity is achieved using the spectra from the nucleolar region alone. Notably, only the nucleolar spectral profiles differentiate the two cancer cell lines. The results point to the importance of the nucleolar regions in diagnostic applications of Raman microscopy as well as further applications in subcellular analysis of cytological processes.

Received 9th June 2015,
Accepted 20th July 2015

DOI: 10.1039/c5an01157d

www.rsc.org/analyst

1. Introduction

Recent decades have seen a notable expansion in exploration of biomedical applications of Raman micro spectroscopy,[1–3] due to the fact that it is a powerful, rapid and non-destructive label-free technique for studying biological systems such as tissue and cells.[4,5]

Raman micro spectroscopy can detect chemical, biological and physical changes of biomolecules, and the specific information contained in the cellular Raman spectrum provides a molecular fingerprint of the sample of interest, which allows Raman micro spectroscopy to differentiate between normal and abnormal cells and tissues, indicating possible applications for example in cancer research.[5,6] Indeed, Raman micro spectroscopy has been shown to provide high specificity and sensitivity, even for pre-cancer detection,[7–10] and is non-invasive and potentially automatable, thus avoiding the disadvantages of many biomedical techniques used to identify and sort cancerous cells from normal ones, which exhibit low specificity and are destructive or perturb the cellular biology.[11–13]

As an optical microscopic technique, Raman micro spectroscopy also has the potential to probe the molecular structure on a cellular and subcellular level.[14,15] In comparison to Infrared absorption spectroscopy; Raman micro spectroscopy offers the possibility to study biological matrices in an aqueous environment due to the weak contribution from water.[16,17] Thus, the potential applications extend beyond disease diagnostics to the label free *in vitro* screening of cytological processes, such as drug or nanoparticle uptake and mechanisms of interaction, and toxicology.[16,18–20] There has

[a]*FOCAS Research Institute, Dublin Institute of Technology, Kevin Street, Dublin 8, Ireland. E-mail: zeineb.farhane@mydit.ie*
[b]*Université François-Rabelais de Tours, Faculty of Pharmacy, EA 6295 Nanomédicaments et Nanosondes, 31 avenue Monge, 37200 Tours, France*
†Electronic supplementary information (ESI) available. See DOI: 10.1039/c5an01157d

been a wide range of studies to date demonstrating the potential of Raman micro spectroscopy to map live and fixed cells with subcellular resolution,[21–25] profile the distribution of anticancer agents[26–30] and nanoparticles in cells[16,31,32] and monitor subcellular processes[33] and toxicological responses.[34–37]

Fundamental to the development of applications of Raman micro spectroscopy for disease diagnostics as well as analysis of cytological processes is an understanding of the variability of the spectral signatures across the subcellular environment, their potential for differentiation of cell phenotype or diseased state, and their sensitivity to external perturbation, such as viral infection, radiation damage, or chemical stress due to, for example, toxic or chemotherapeutic agents. It is clear that the signatures for the cytoplasm, nucleus and nucleoli are distinct and differentiable,[38] but it is not clear which region has the best diagnostic potential or sensitivity to external insult. The current study examines the subcellular basis of differentiation of human cell lines *in vitro*, both normal and cancerous, using Raman micro spectroscopy.

Numerous studies over the last few years have investigated the capability of Raman micro spectroscopy to differentiate between cancerous cell lines; Crow *et al.*[39] used human prostate cancer cell lines, Pijanka *et al.* investigated lung cancer cell lines,[40] and Chan *et al.* explored neoplastic hematopoietic cells,[11] while Krishna *et al.* were interested in mixed cell populations of human promyelocytic leukemia and breast cancer.[41] All those studies demonstrated that Raman micro spectroscopy, coupled with multivariate statistics, is able to distinguish between different cell lines with a high specificity and sensitivity. However, the basis of the differentiation was not elucidated in terms of the subcellular regions.

In this study, Raman profiles of three cell lines from same anatomical origin, the human lung, were compared and analysed. The first part is the investigation of the differentiation of a normal human bronchial epithelium cell line, BEAS-2B, from the adenocarcinoma human alveolar basal epithelial cell line, A549, and the non-small-cell lung cancer cell line Calu-1. Thereafter, the two cancer cell lines are compared to each other, using Raman micro spectroscopy. The morphological and topographical characteristics of the two human lung cancer cell lines A549 and Calu-1, using Flow Cytometry, CLSM and AFM were also analysed and correlated to their Raman spectroscopic features.

In all cases, spectral profiles of the cytoplasm, nucleus and nucleoli were independently acquired and analysed, and the study highlights the importance of the nucleoli in potential diagnostic and bioanalytical applications.

2. Materials and methods

2.1. Materials

A549 human lung adenocarcinoma cells with the alveolar type II phenotype, and BEAS-2B normal human bronchial epithelium (ATCC® CRL-9609™), virus transformed, infected with a replication-defective SV40/Adenovirus 12 hybrid and cloned, were all obtained from ATTC (Manassas, VA, USA). Calu-1 human lung epidermoid cells were obtained from the European Collection of Cell Cultures.

SYTO® Green Fluorescent Nucleic Acid Stains and Wheat Germ Agglutinin conjugates (WGA), a cell membrane glycoconjugates binder, purchased from BioSciences (Ireland, suppliers for Life Technologies), were employed to image the nuclear compartment and cytoplasmic membrane of cells using Confocal Laser Scanning Microscopy.

2.2. Cell culture

A549 and BEAS-2B cells were cultured in DMEM (with 2 mM L-glutamine) and Calu-1 in RPMI, all with 10% foetal bovine serum (FBS) at 37 °C in an humidified atmosphere containing 5% CO_2 and cells were split every two days to maintain ~60% confluence.

2.3. Sample preparation and measurement protocols

2.3.1. Raman micro spectroscopy. Cells ~5000 were seeded and incubated on CaF_2 windows (Crystan Ltd, UK) for 48 h in order to achieve a final number of approximately 10^4 cells. Medium was removed and samples were rinsed twice with sterile PBS then fixed using formalin (4%, 15 mn) and spectra were recorded after air drying in ambient atmosphere.

A Horiba Jobin–Yvon LabRAM HR800 spectrometer with a 785 nm, 300 mW diode laser as source, Peltier cooled 16-bit CCD, 300 lines per mm grating and 100 μm confocal hole, was used for this work. Spectra were acquired from the three cell locations: cytoplasm, nuclear and nucleolar in the range from 400 cm^{-1} to 1800 cm^{-1} with an ×100 objective (LCPlanN, Olympus) for 30 s two times, to finally produce a data set of 30 points per cell location for each cell line, over a total of 90 different cells.

2.3.2. Confocal laser scanning fluorescence microscopy (CLSM). Samples were prepared on uncoated glass bottom Petri dishes (MatTek Corporation, USA). Approximately 10^4 Cells were allowed to attach for two hours, then covered with cell culture medium. After incubation, the medium was removed and samples were rinsed twice with sterile PBS and fixed in formalin (4%, 15 mn).

After fixation, samples were washed with Hank's balanced salt solution (HBSS) and WGA (7.5 μL of WGA per 1 mL HBSS) was first added and cells were incubated for 20 min and washed with HBSS. Sytox® green nucleic acid stain (2 μL per 1 mL of HBSS) was thereafter added, cells were incubated for 30 min and washed with HBSS then imaged in HBSS.

Confocal Laser Scanning microscopic images were recorded using an inverted Zeiss LSM 510 confocal laser scanning microscope equipped with a ×60 oil immersion objective. Excitation wavelengths used were 488 nm for Sytox® green nucleic acid stain (emission wavelength 523 nm) and 633/647 nm excitation/emission for WGA.

2.3.3. Flow cytometry. Cells were cultured in T75 flasks over 48 h and then trypsinised and centrifuged in 10 mL fresh medium at 4 °C and 1000 rpm for 5 min. After this, the cells

were re-suspended with 5 mL PBS and only 2 mL was used for analysis. Samples were prepared in parallel and the two cell lines were analysed separately. A total number of 2×10^4 cells was analysed for each sample. The experiments were conducted in triplicate (three independent experiments).

Flow cytometry analysis was performed using a BD Biosciences Accuri C6 Flow Cytometer (Becton Dickinson, Oxford, UK) without any dyes.

2.3.4. Atomic force microscopy (AFM). The air dried samples on CaF_2 substrates were profiled using a MFP-3D BIO AFM (Asylum Research). The cantilevers used were Olympus silicon AC240. Tips were 160 nm long and had a typical resonant frequency of 70 kHz. The AFM was operated in AC mode in order to minimize tip/sample interaction. Typical free air amplitudes were ~200 mV and a high amplitude set-point relative to the set-point was maintained to minimize sample damage. The images obtained, from 5 to 10 cells per cell line, contained 1024 pixels per scan line and only one representative image of typical cell for each cell line is shown.

2.4. Data analysis

Raman spectra pre-processing and analysis were performed in Matlab 2013 using algorithms developed in house.

Prior to analysis, spectra were smoothed (Savitsky–Golay filter 5th order, 7 points), baseline corrected, substrate background subtracted, using a polynomial method home developed, and vector normalised.

After pre-processing, PCA (principal components analysis) and PCA-Linear Discriminants Analysis (PCA-LDA), powerful approaches commonly used for the analysis of large spectral data sets, were employed as supervised multivariate analysis tools to differentiate the data recorded from different subcellular localisations and cell lines. PCA allows the reduction of the number of variables in a multidimensional dataset, the order of the PCs denoting their importance in the dataset where PC1 describes the highest amount of variation.[18,20] While PCA identifies differences between the data sets, LDA maximizes these differences so as to group similar spectral sets. PCA performs a feature reduction of the data and LDA classifies the data into one of two or more classes. Thus, if a group of spectra have a similar correlation to the shape defined by PC1 and that defined by PC2; they are classified as same class.

PCA was performed on each of the datasets independently (nucleoli, nucleus, and cytoplasm). LDA was then performed on each of the datasets scores independently and a 10-fold cross validation was performed to produce confusion matrices.[42,43] LDA accuracy was calculated using a 10-fold cross validation on increasing numbers of latent variables (PC scores) for the classification of all cancer types and normal cells. The classification which resulted in the maximum accuracy while keeping the number of latent variables to a minimum was chosen for all successive models. In the case of the classification of all cancer cells and normal one, from a plot of accuracy as a function of increasing number of latent variables, the maximum accuracy was found when 4 principal components were used in the classification. Further addition of principal components only increased the complexity of the model without further improving the performance.

The Accuri Flow cytometry software was used for the initial analysis of flow cytometry samples, but the Beckman Coulter Summit software and the FCS Express Research Edition have been used for the reanalysis of the samples. The QC control of the instrument was performed using Spherotech 6 and 8 peak beads.

3. Results and discussion

3.1. Raman micro spectroscopy

Raman spectra were taken from the three cell compartment for all cell lines and Fig. 1 shows the average spectra corresponding to each cell region for Calu-1 cells. Visibly, it can be seen that the mean spectra of the nucleolar, nuclear and cytoplasmic regions are somewhat different, and discriminating peaks (indicated by highlighted regions in Fig. 1) at, for example, 1578, 1095, 830 and 795 cm^{-1} can be allocated to nucleic acids which correspond respectively to vibrations of the DNA bases adenine and guanine, DNA PO_2^- symmetric stretching, ribose phosphate and DNA backbone O–P–O stretching,[44,45] while others at 1300 (CH deformation) and 717 cm^{-1} (CN + $(CH_3)_3$ stretching) are associated with lipid components of the cell membrane, which are also observable in subsequent spectra of the nuclear and nucleolar regions, although more prominently in the spectra of the cytoplasmic region. The DNA bands at 1095 cm^{-1} and 830 cm^{-1} indicate that the DNA is in B form and one at 813 cm^{-1} corresponds to DNA A form.[17]

Similar profiles were obtained for the subcellular analysis of A549 cells.

For a more detailed understanding of the differences in spectral profiles of the subcellular regions, a multivariate analysis is more informative, and therefore, PCA was employed to analyse and compare the spectral profiles of the subcellular regions as well as the differences between cancer and normal cell lines. Figures representing the differentiation of the

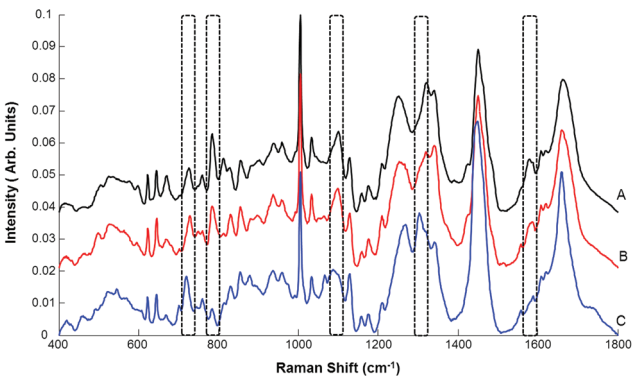

Fig. 1 Mean spectra of nucleolus (A), nucleus (B) and cytoplasm (C) of Calu-1 cell line. Highlighted regions indicate discriminatory features.

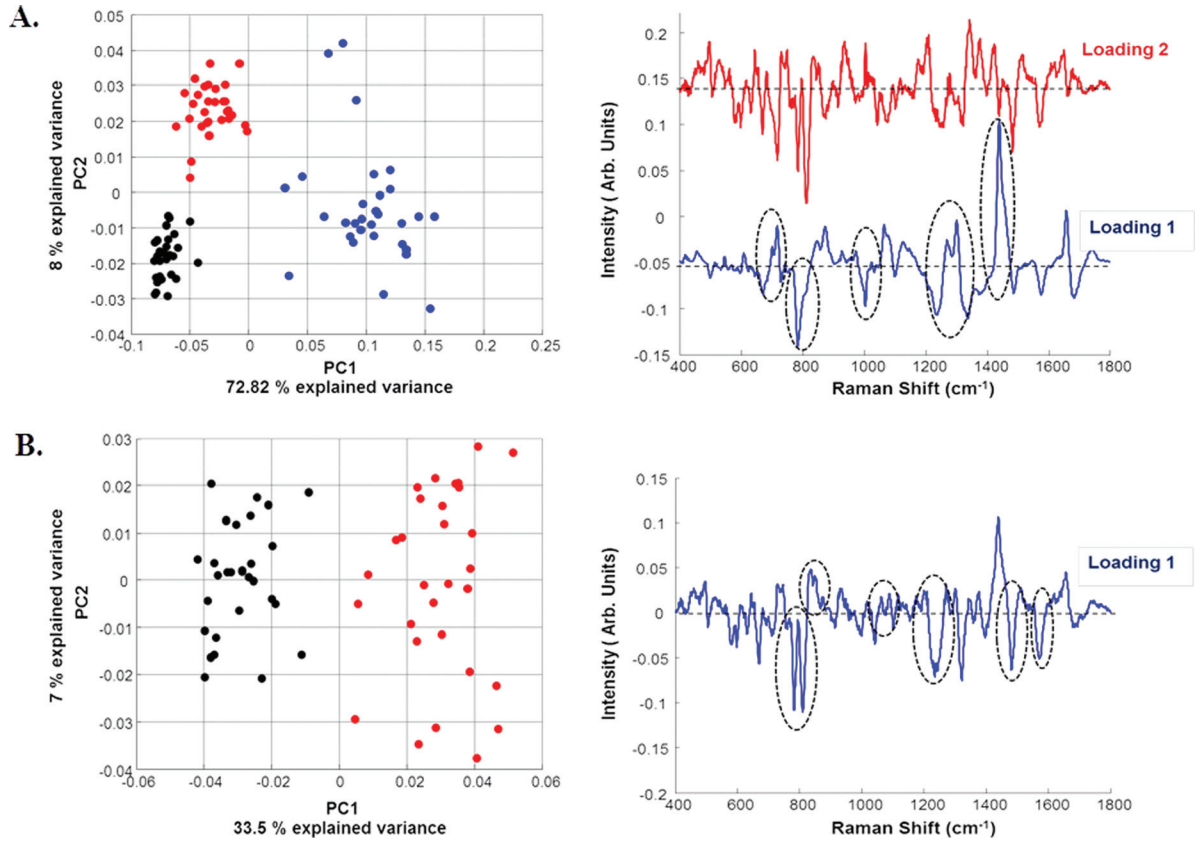

Fig. 2 A. PCA scatter plot of nucleolar, nuclear and cytoplasmic regions of Calu-1 cells, with corresponding loadings of PC1 and PC2. B. PCA of nucleolar and nuclear regions of Calu-1 cells and corresponding loading of PC1. ● Cytoplasm, ● Nucleus, ● Nucleolus.

spectra by PCA according to the corresponding PC loadings were plotted and, for clarity, in all PCA figures, the loadings are off set, the dashed horizontal line in all cases indicating zero loading.

As an illustration of the analysis technique used throughout, Fig. 2A shows the PCA scatter plot of the cytoplasmic, nuclear and nucleolar spectra of the Calu-1 cell line, along with the corresponding loadings of PC1 and PC2. PC1 clearly differentiates between the cytoplasmic and integrated nuclear regions (nuclear and nucleolar) and, according to the corresponding loading (loading 1), the most visible discriminant features derive from DNA, 795 cm^{-1} and 1095 cm^{-1}, related to DNA form and DNA PO_2^- symmetric stretching, and lipids at 717 cm^{-1} (CN + $(CH_3)_3$ stretching), 1300 (CH_2 stretching) and 1440 cm^{-1} (CH stretching). The differentiation of the subcellular regions according to PC1 is not unexpected, due to the significant biochemical differences between the combined nuclear and cytoplasmic regions which are similar for all cell lines.

Although some degree of discrimination of the nuclear and nucleolar regions according to PC2 is evident in Fig. 2A, a better visualisation of this is achieved by a direct pairwise PCA of the two datasets, as shown in Fig. 2B. PC1 now clearly differentiates the nucleolar and nuclear regions. It exhibits discriminating negative peaks related to nucleoli at 782 and 1336 cm^{-1} (Uracil, Cytosine and Thymine) corresponding to RNA,[46] 1242 cm^{-1} (Amide II), 1480 cm^{-1} (Guanine, Adenine) and 1578 cm^{-1} (proteins) due to the contribution of surrounded membrane, as well as positives ones at 728 (Adenine), 830 cm^{-1} (O–P–O asymmetric stretching) and 1095 cm^{-1} (DNA PO_2^- symmetric stretching), corresponding to the nuclear region, which is the primary location of DNA, while the nucleolar regions contain RNA and a small quantities of DNA.[4,38] Similar differentiation can be achieved for the subcellular regions of A549 cells (data not shown).

In a similar fashion, PCA was employed to compare the spectral profiles of the normal lung human cell line BEAS-2B to the two lung cancer cell lines A549 and Calu-1.

The PCA scatter plot of Fig. 3A compares the three subcellular regions of all three lung cell lines. PC1 largely differentiates between the cytoplasmic regions and the integrated nuclear and nucleolar regions of the cells, and the corresponding loading exhibit features related to nucleic acid (DNA and RNA) and lipids, similar to the loading of PC1 in Fig. 2A.

Accounting for 21% of the explained variance, PC2 indicates a clear differentiation between the normal cell line and the two cancerous ones. Although the loading of PC2 represents differentiating features of all three subcellular regions, identifiable features include negative peaks at 669 (Thymine and Guanine), 728 (Adenine), 1095 cm^{-1} (DNA PO2-symmetric

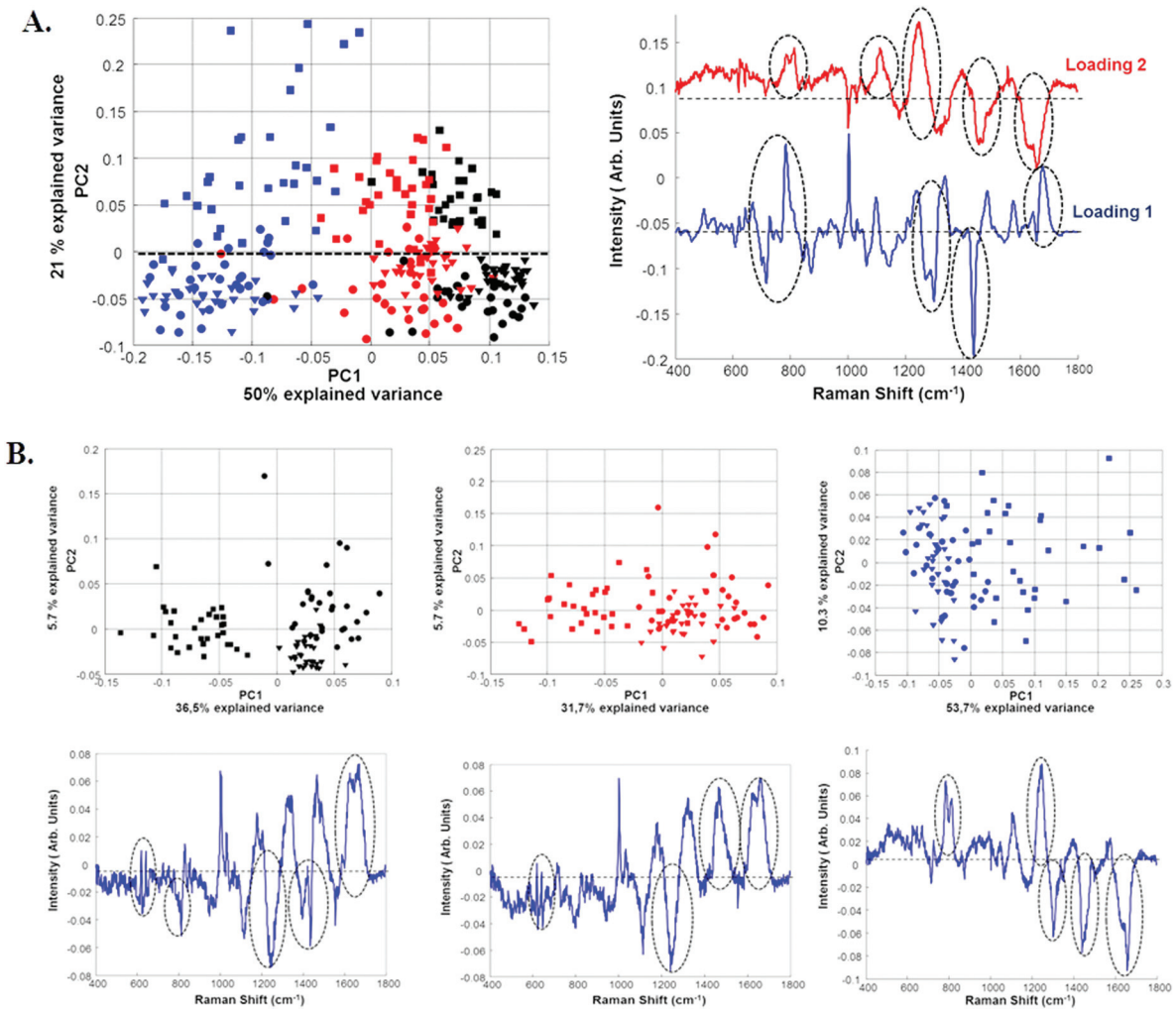

Fig. 3 PCA of nucleolar, nuclear and cytoplasmic regions of A. A549, Calu-1 and BEAS-2B with corresponding loadings of PC1 and PC2. B. PCA of each cell localisation for A549, Calu-1 and BEAS-2B and the corresponding loadings of PC1. Cytoplasm ● Nucleus ● Nucleolus ● A549 cell line; Cytoplasm ▼ Nucleus ▼ Nucleolus ▼ Calu-1 cell line; Cytoplasm ■ Nucleus ■ Nucleolus ■ BEAS-2B cell line.

stretching) and ones at 1005 (Phenylalanine), 1320 (Guanine), 1440 (Guanine and Adenine), and 1665 cm^{-1} (Amide I), associated with the cancer cell lines. Positive peaks corresponding to lipids at 760 and 820 (tryptophan ring), 1115 (C–C stretching), 1250 and 1420 cm^{-1} (lipids C═C and C–H vibration) are associated with the normal cell line. A similar scatterplot and loadings profile, with separation between integrated nuclear region and cytoplasmic area according to PC1 and differentiation of normal and cancer cell line according to PC2 is observable when cell lines were analysed pairwise, A549 *versus* BEAS-2B and Calu-1 against BEAS-2B (Fig. S1, ESI†).

The PCA discriminating features between normal and cancer cells correspond to DNA and proteins for cancer cell lines and lipids for the normal one, which is consistent with the fact that cancerous cells have a more active metabolism and exhibits more proteins and more DNA than normal cells but present less cytoplasm and therefore lipids are positive discriminating features for normal cells.

The differentiation of the cell lines is more evident when the subcellular regions are analysed independently using PCA, as shown in Fig. 3B. The normal and cancerous cell lines are now largely discriminated by PC1 and almost the same discriminating features can be found in the loadings of PC1 for the nucleolar and nuclear regions, while additional peaks in the loading of PC1 for the cytoplasm of the normal *versus* cancerous cells are observed at 760 and 820 (tryptophan ring) and 1250 (Amide III), related to normal cells and ones at 717 (CN + $(CH_3)_3$ stretching), 1400 (CH deformation) and 1578 cm^{-1} (protein) 1661 cm^{-1} (lipids C═C stretching) related to cancerous cell lines.[4,17,30,47]

Thus using PCA allows a separation between normal and cancerous cell lines. Notably, however, no differentiation of the cancerous cell lines is evident. To investigate this further, the cancer cell lines were compared to each other and spectra from the nucleolus, nucleus and cytoplasm were similarly analysed.

As shown in Fig. 4A, a scatter plot of the combined PCA of the nucleolar, nuclear and cytoplasmic regions of the A549, Calu-1 cancer cell lines, there is no clear separation between the two cells. As before, PC1 differentiates between the cytoplasmic and combined subcellular regions, but, in contrast to the comparison of the normal and cancerous cell line, there is no clear differentiation between the two cell lines. Indeed, PC1 discriminates between the cytoplasm and the combined

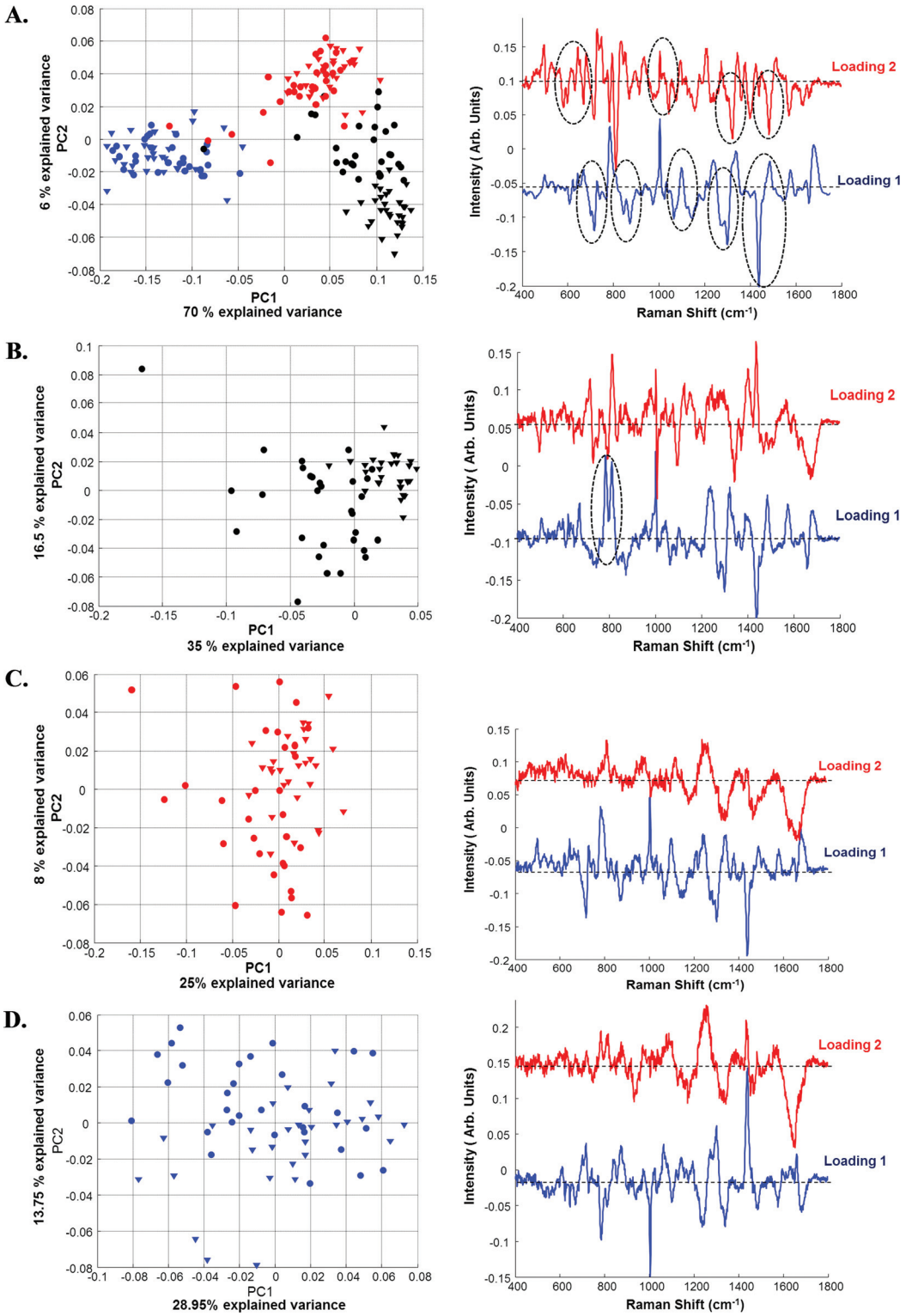

Fig. 4 PCA scatterplots and corresponding loadings of PC1 and PC2 of A549 and Calu-1 cells: A. nucleolus, nucleus and cytoplasm B. nucleolus, C. nucleus D. cytoplasm. Cytoplasm ● Nucleus ● Nucleolus ● A549 cell line; Cytoplasm ▼ Nucleus ▼ Nucleolus ▼ Calu-1 cell line.

nuclear region, for both cell lines and the corresponding loading exhibits features corresponding to lipids, 717 and 873 cm^{-1} (CN^+ $(CH_3)_3$, 1270 and 1303 cm^{-1} (C–H vibrations) and 1450 (CH_2 deformation) and ones related to DNA at 784 (Cytosine and Thymine), 1095 (DNA $PO2^-$ symmetric stretching) and 1578 cm^{-1} (Guanine, Adenine). PC2 partially discriminates the nucleolar and nuclear regions and exhibits discriminating negative peaks for the nucleolar region at 784 and 1336 cm^{-1} (Uracil, Cytosine and Thymine) corresponding to RNA, 1242 cm^{-1} (Amide II), 1480 cm^{-1} and 1578 cm^{-1} (Guanine, Adenine), as well as positives ones at 728 (Adenine), 830 cm^{-1} (O–P–O asymmetric stretching) and 1095 cm^{-1} (DNA PO_2^- symmetric stretching), corresponding to the nuclear region.[4,38]

Therefore it appears that Raman micro spectroscopy is unable to differentiate between cancerous cells, although it is able to distinguish the subcellular regions for all cell lines.

Nevertheless, previous studies, have demonstrated the ability of Raman micro spectroscopy to distinguish between different cancer cell lines.[8,11,28,40,48,49] To explore the apparent discrepancy in results, the individual subcellular regions were further analysed (Fig. 4B–D).

Results shows no indication of discrimination between the two lung cancerous cells for the nuclear and cytoplasmic areas (Fig. 4C and D) although there is some degree of differentiation according to PC1 (35% of variation) for the nucleolar regions of A549 and Calu-1 (Fig. 4B). Discriminant features of the loading of PC1 include negative peaks at 1270 (RNA Uracil and cytosine ring stretching), 1320 and 1450 (CH_2 deformation) and 1661 cm^{-1} (Lipids C=C stretching). The same features are found to be higher in the mean spectra of nucleolar A549 compared to Calu-1 (Fig. 5), indicating that there are more lipids in the former. Also prominent in the loading of PC1 are also two strong positive peaks at 784 cm^{-1} (Uracil, Cytosine and Thymine) and 811 cm^{-1} (RNA O–P–O phosphodiester bond) as well as ones at 1240 (Amide III), 1480 and 1578 cm^{-1} (Guanine, Adenine), which indicate that there is a stronger RNA contribution in Calu-1 cells than A549. This can be clearly seen in the mean nucleolar spectra in Fig. 5.

Moreover, according to the mean spectra, it seems that the most notable differences in nuclear and nucleolar regions between A549 and Calu-1 corresponds to the features at 813 cm^{-1} (DNA A form) and at 830 cm^{-1} (DNA B form). The ratio between to the two peaks (enlargement Fig. 5) is inverted which signifies that there is more DNA B form in A549 than in Calu-1 and *vice versa*.

To support Raman micro spectroscopy observations, Confocal Laser Scanning Microscopy, Flow Cytometry and Atomic Force Microscopy were in their turn employed to compare the two human lung cancer cell lines.

3.2. Confocal laser scanning fluorescence microscopy (CLSM)

CLSM was employed in order to identify the morphological characteristics of the two cell lines, A549 and Calu-1. As shown in Fig. 6, before and after nucleic and cytoplasmic staining, the two cell lines present a different shape and size, as well as numbers of nucleoli, which are clearly resolved within the nucleus and have diameters ~2–4 μm. Indeed, WGA, a cytoplasmic membrane stain which delimits the cytoplasmic membrane, highlights the shape of cells and shows that Calu-1 are bigger and longer than A549 cells, while Sytox® green, a specific nuclear dye which has a high affinity for DNA, shows that Calu-1 cells present a higher density of nucleoli and a larger nuclear area than A549 cells.

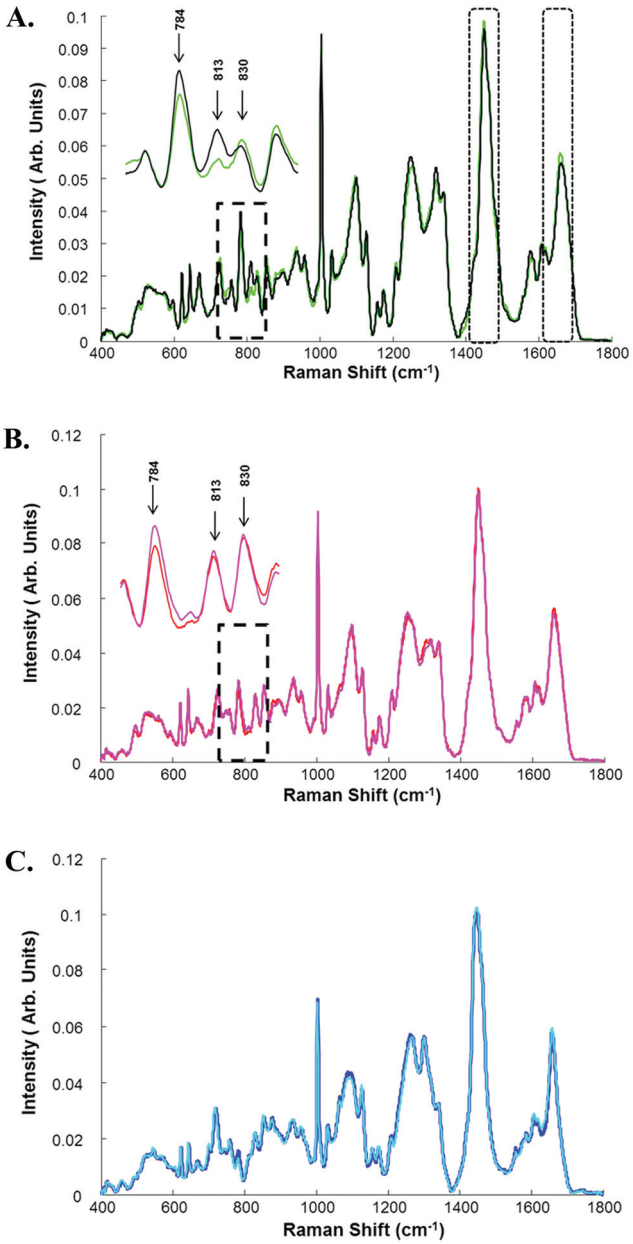

Fig. 5 Mean spectra of A. nucleolus of A549 (green) and Calu-1 (black), B. nucleus of A549 (red) and Calu-1 (magenta) and C. cytoplasm of A549 (blue) and Calu-1 (cyan).

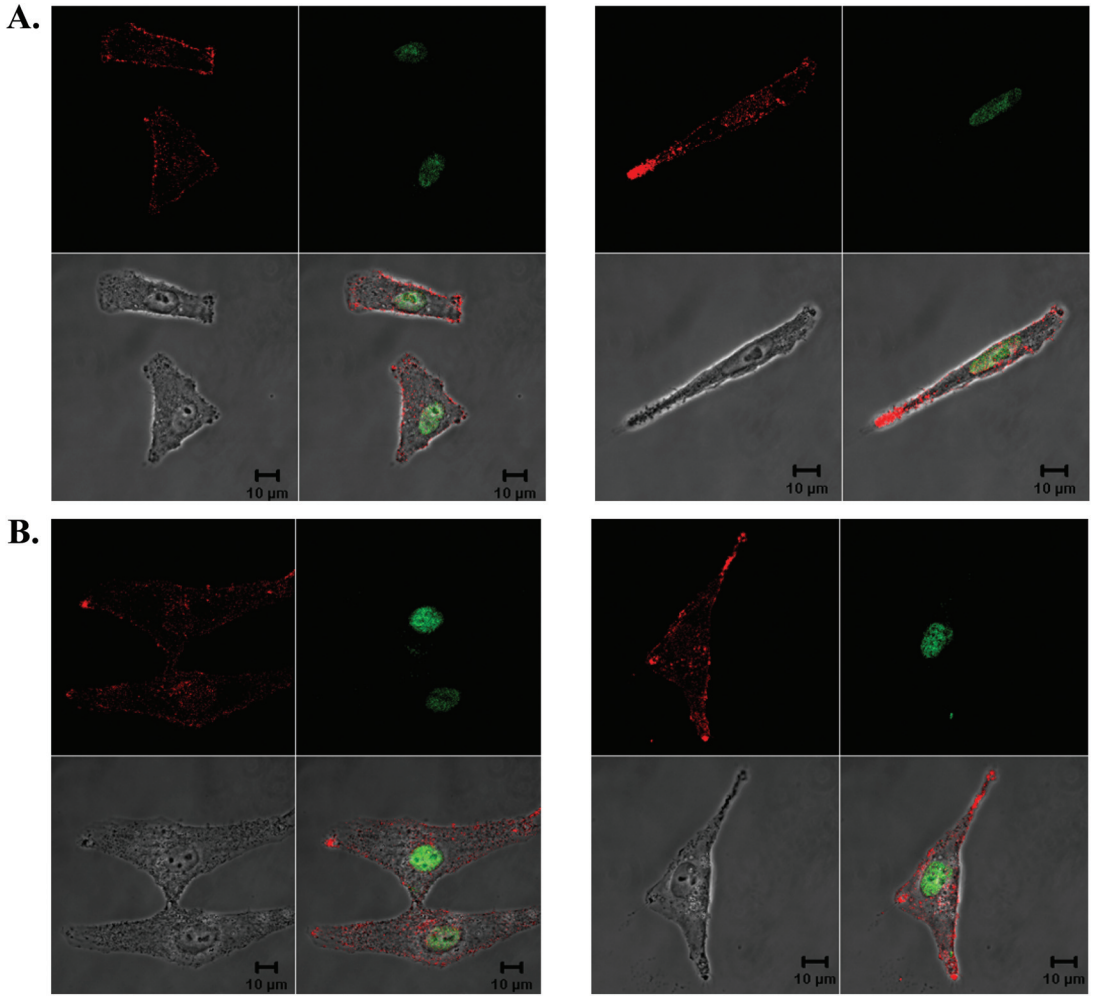

Fig. 6 Confocal fluorescence images of A. A549 and B. Calu-1 stained with Sytox® green nucleic acid stain and WGA.

3.3. Flow cytometry

As shown in Fig. 7, the flow cytometry 2D scatter plots are different from one cell line to another, indicating that Calu-1 cells are more spread and bigger in size than A549. This is confirmed in the histograms; Calu-1 (red) and A549 (green) show a difference in cell surface and size (FSC forward scatter) and cell granularity and internal environment (SSC side scattering) between the two cell lines, confirming that Calu-1 cells present larger size and dispersive granularity of the nucleus, which explains the most significant percentage of cellular side scattering,[50] than A549, consistent with the confocal microscopy results.

3.4. AFM

AFM shows that both cell lines have different topography. Indeed, according to Fig. 8 A549 cells are higher and more convex than Calu-1 (Height 1.4 μm for A549 compared to 1.2 μm for Calu-1). Additionally, it can be seen from the structure of the height profiles that Calu-1 cells have more surface granularity, consistent with larger number of nucleoli, which confirms the CLSM and flow cytometry results.

According to Flow Cytometry (SCC maximum 500 000 for A549 and 1 000 000 for Calu-1) and AFM (Fig. 7 and 8), A549 cells are thicker than Calu-1 but present fewer and smaller nucleoli, which is confirmed by CLSM. Nucleoli size for both cell lines is by the order of 2–4 μm, larger than the Raman laser spot (1 μm) and, according to Raman micro spectroscopy; RNA is more prominent in Calu-1 nucleoli than those of A549.

3.5. PCA-LDA

Thus, CLSM, Flow Cytometry and AFM show that A549 and Calu-1 cells are different in size, morphology and topography. Raman micro spectroscopy was unable to differentiate between them with high sensitivity according to the biochemical fingerprint of the cytoplasmic or nuclear regions alone. However, differentiation of cell lines is achievable according to the spectroscopic signature of the nucleoli.

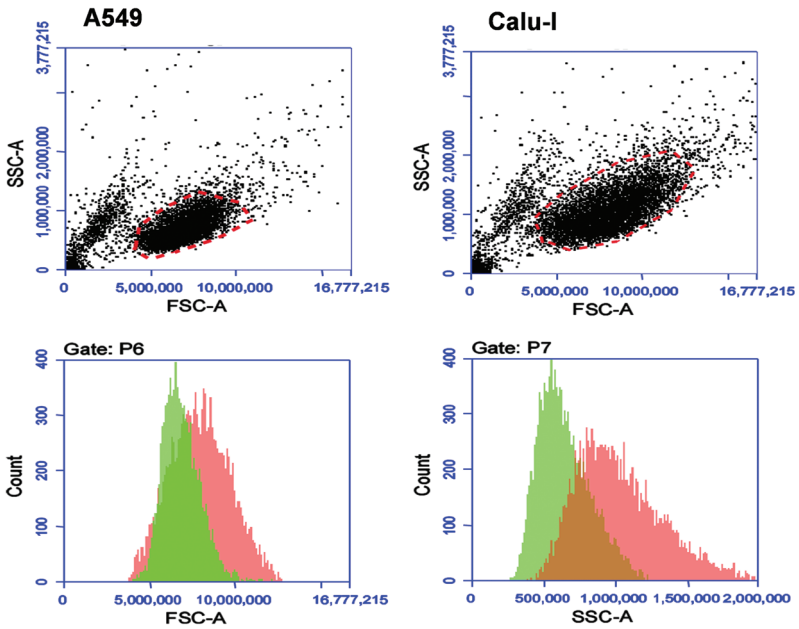

Fig. 7 Flow cytometry 2D scatter plots (FSC *vs.* SSC) with debris excluded and histograms ((FSC *vs.* cell number) and (SCC *vs.* cell number)) for both cancer cell lines A549 (green) and Calu-1 (red).

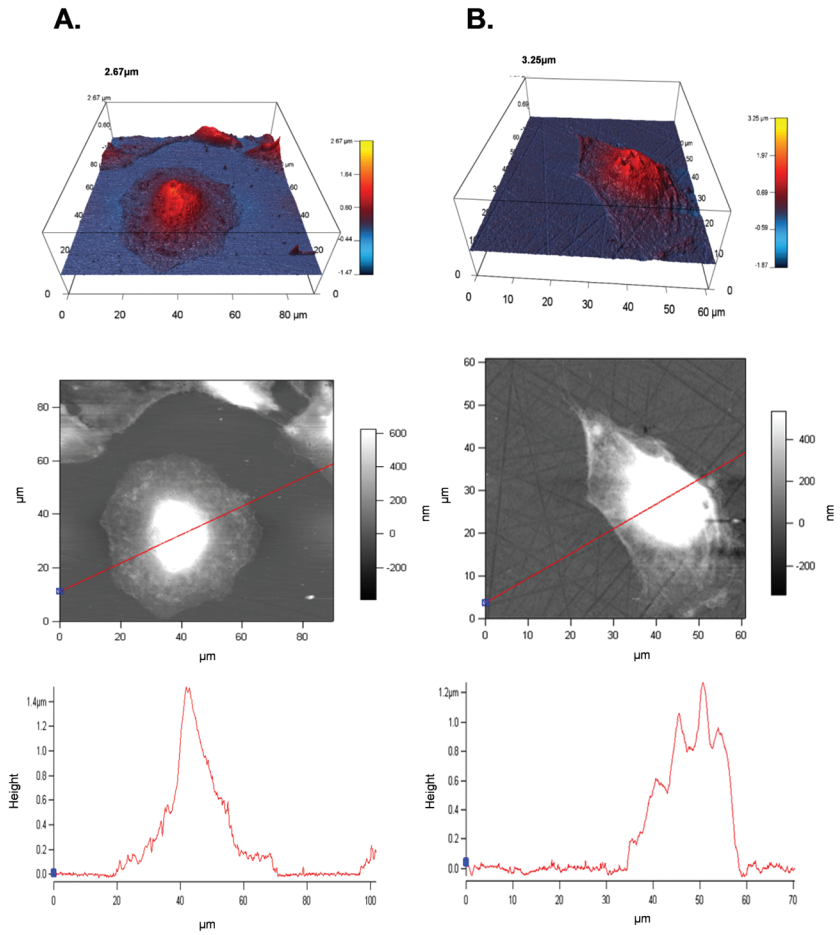

Fig. 8 AFM images of A. A549 and B. Calu-1: 3D image, height scan and topographical profile generated for height scan; respectively.

Table 1 Confusion matrix table for A549, Calu-1 and BEAS-2B. A. nucleolus + nucleus, B. nucleolus, C. nucleus and D. cytoplasm

	A549	Calu-1	BEAS-2B
A.			
A549	40	18	2
Calu-1	16	43	1
BEAS-2B	2	3	55
Sensitivity %	68.9	78.1	94.8
Specificity %	52.3	52.7	91.9
B.			
A549	26	4	0
Calu-1	1	29	0
BEAS-2B	0	0	30
Sensitivity %	96.2	87.8	100
Specificity %	87.8	96.2	100
C.			
A549	19	9	2
Calu-1	6	23	1
BEAS2B	1	4	25
Sensitivity %	73.1	63.8	89.2
Specificity %	67.6	70.8	84.3
D.			
A549	23	7	0
Calu-1	14	16	0
BEAS-2B	4	1	25
Sensitivity %	56.1	66.6	100
Specificity %	63.1	61.1	83.3

Nucleoli are non-membrane-bound nuclear compartments, well described and analysed in details since the last millennium.[51,52] They are responsible for ribosome biogenesis and diverse cellular functions and processes such as cell cycle control, cellular stress response, nuclear export and sequestration of key proteins regulators of cell-cycle activity and response to apoptosis and early stage cellular response to toxic such as chemotherapeutic drugs.[30] The size, number and organisation of nucleoli are cell-specific and nuclear proteins, notably histone, play an important role in the nucleoli stability and functions.[53,54]

The important role played by nucleoli and its cell specificity explain the fact that it is spectroscopically the discriminant factor between cancer cell lines. For confirmation, PCA was coupled with LDA and confusion matrices were generated using 4 principal components and, in the first instance, nucleolar and nuclear areas were analysed in combination. The results shown in Table 1A indicate a sensitivity and specificity of between 40 and 60% for the two cancerous cell lines and 91.8% specificity and 93.2% specificity for the normal cells, BEAS-2B, which confirms, along with the LDA plot in Fig. 9, that poor discrimination between the cancerous cell lines is achievable. To improve the specificity and sensitivity, the nucleolar and nuclear regions were analysed separately.

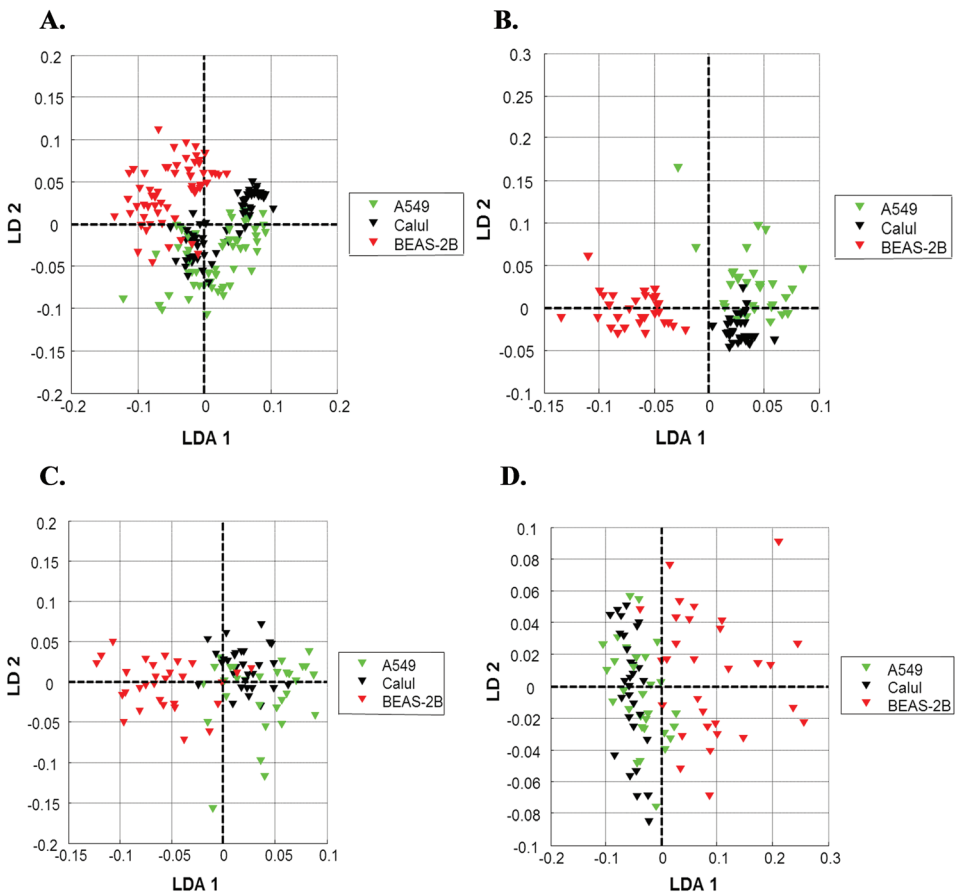

Fig. 9 PCA – LDA of subcellular regions of A549, Calu-1, and BEAS-2B. A. nucleolar + nuclear, B. nucleolar, C. nuclear and D. cytoplasm.

It is notable that in the confusion matrix of Table 1B, for the nucleolar regions of BEAS-2B, the sensitivity and specificity are 100% (separation is obvious in Fig. 9B). A clearly better separation for the two cancerous cell lines is achievable for the nucleolar region, and a similar amelioration can be observed for the nuclear region (Table 1C), although the specificity and sensitivity remains lower than that of the nucleolar region. Significantly lower sensitivities and specificities were obtained for the cytoplasmic regions of the cancer cell lines (Table 1D). The results are supported by the PCA-LDA plot in Fig. 9.

In summary, Raman micro spectroscopy coupled with both PCA and PCA-LDA highlights the critical importance of nucleoli in determining the biochemical identity of the cell. Recent studies using Raman micro spectroscopy to investigate the nucleoli biochemical and molecular composition, and differences in this nuclear compartment between normal and cancer cell lines, highlighted the potential role of the nucleoli in cell differentiation[55,56] The current study confirms that this nuclear organelle, in addition to its essential cellular function, is also the primary source of the differentiating Raman spectroscopic fingerprint of the cell lines. Notably, the improved differentiation of the cell lines based on the spectral profiles of the nucleoli alone does not consider the additional discriminating factor of the number and or density of nucleoli in the nucleus of different cell lines. In studies which compare an integrated spectral analysis of the nucleus of the cell,[34] this factor will amplify the intrinsic biochemical differences of the nucleoli of different cell lines. The study points towards the importance of the nucleoli in the diagnostic potential of Raman micro spectroscopy. The role of the nucleoli in the early stage response of cells to chemotherapeutic agents has also been demonstrated,[27] indicating the sensitivity of the spectral profile of this subcellular region to cytological processes.

4. Conclusion

While this study confirms the ability of Raman micro spectroscopy to differentiate between normal and cancerous cell lines *in vitro*, as well as between cancer cell-lines from the same anatomical site, it clearly demonstrates that the discriminating potential varies depending on the subcellular region analysed. As, typically, the sampled spot size in Raman micro spectroscopy is less than the cell area, this has important implications for optimisation of diagnostic potential in cytopathology, but also for the sensitivity of analysis of cellular processes such as the action of chemotherapeutic agents.

A comparison of normal and cancer cell lines indicates that all subcellular regions are differentiable. However, the classification sensitivities and specificities are lowest for the cytoplasmic regions. While somewhat improved classification is achievable using the spectra of the integrated nuclear region, classification based on the nucleolar regions alone is significantly superior. Notably, in the detailed spectral analysis, the cancer cell lines were only well differentiated on the basis of the nucleolar regions.

The morphological analysis demonstrates that the cells differ significantly in their nucleolar content, while the spectroscopic study indicates significant differences in the individual nucleolar biochemical content. The study demonstrates the importance of the nucleoli in its contribution to the diagnostic potential of Raman micro spectroscopy as well as further applications in subcellular analysis of cytological processes.

Acknowledgements

This work was supported by Science Foundation Ireland Principle Investigator Award 11/PI/1108.

The authors thank Dr Josep Sulé-Suso, Institute for Science & Technology in Medicine, Keele University, Guy Hilton Research Centre UK and Cancer Centre, Royal Stoke University Hospital, University Hospitals of North Midlands, UK, for providing the Calu-1 cell line.

References

1 A. Downes and A. Elfick, *Sensors*, 2010, **10**, 1871–1889.
2 C. Krafft and J. Popp, *Anal. Bioanal. Chem.*, 2015, **407**, 699–717.
3 M. Diem, M. Miljkovic, B. Bird, T. Chernenko, J. Schubert, E. Marcsisin, A. Mazur, E. Kingston, E. Zuser, K. Papamarkakis and N. Laver, *Int. J.*, 2012, **27**, 34.
4 Z. Movasaghi, S. Rehman and I. U. Rehman, *Appl. Spectrosc. Rev.*, 2007, **42**, 493–541.
5 J. Chan, S. Fore, S. Wachsmann-Hogiu and T. Huser, *Laser Photon. Rev.*, 2008, **2**, 325–349.
6 K. Kong, C. Kendall, N. Stone and I. Notingher, *Adv. Drug Delivery Rev.*, 2015, DOI: 10.1016/j.addr.2015.03.009, Accepted manuscript March 2015.
7 C. Kallaway, L. M. Almond, H. Barr, J. Wood, J. Hutchings, C. Kendall and N. Stone, *Photodiagn. Photodyn. Ther.*, 2013, **10**, 207–219.
8 N. Rashid, H. Nawaz, K. W. C. Poon, F. Bonnier, S. Bakhiet, C. Martin, J. J. O'Leary, H. J. Byrne and F. M. Lyng, *Exp. Mol. Pathol.*, 2014, **97**, 554–564.
9 C. Kendall, J. Day, J. Hutchings, B. Smith, N. Shepherd, H. Barr and N. Stone, *Analyst*, 2010, **135**, 3038–3041.
10 N. S. Eikje, K. Aizawa and Y. Ozaki, in *Biotechnology Annual Review*, ed. M. R. El-Gewely, Elsevier, 2005, vol. 11, pp. 191–225.
11 J. W. Chan, D. S. Taylor, T. Zwerdling, S. M. Lane, K. Ihara and T. Huser, *Biophys. J.*, 2006, **90**, 648–656.
12 C. Knipfer, J. Motz, W. Adler, K. Brunner, M. T. Gebrekidan, R. Hankel, A. Agaimy, S. Will, A. Braeuer, F. W. Neukam and F. Stelzle, *Biomed. Opt. Express*, 2014, **5**, 3252–3265.

13 T. Huser and J. Chan, *Adv. Drug Delivery Rev.*, 2015, DOI: 10.1016/j.addr.2015.06.011, Accepted manuscript 26 June 2015.
14 F. Bonnier, P. Knief, B. Lim, A. D. Meade, J. Dorney, K. Bhattacharya, F. M. Lyng and H. J. Byrne, *Analyst*, 2010, **135**, 3169–3177.
15 M. Miljkovic, T. Chernenko, M. J. Romeo, B. Bird, C. Matthaus and M. Diem, *Analyst*, 2010, **135**, 2002–2013.
16 J. Dorney, F. Bonnier, A. Garcia, A. Casey, G. Chambers and H. J. Byrne, *Analyst*, 2012, **137**, 1111–1119.
17 I. Notingher, S. Verrier, H. Romanska, A. E. Bishop, J. M. Polak and L. L. Hench, *Spectroscopy*, 2002, **16**, 43–51.
18 G. Romero, Y. Qiu, R. A. Murray and S. E. Moya, *Macromol. Biosci.*, 2013, **13**, 234–241.
19 C. Matthäus, T. Chernenko, J. A. Newmark, C. M. Warner and M. Diem, *Biophys. J.*, 2007, **93**, 668–673.
20 J. Ling, S. D. Weitman, M. A. Miller, R. V. Moore and A. C. Bovik, *Appl. Opt.*, 2002, **41**, 6006–6017.
21 A. F. Palonpon, M. Sodeoka and K. Fujita, *Curr. Opin. Chem. Biol.*, 2013, **17**, 708–715.
22 S. Caponi, L. Liguori, A. Giugliarelli, M. Mattarelli, A. Morresi, P. Sassi, L. Urbanelli and C. Musio, *Biophys. Chem.*, 2013, **182**, 58–63.
23 A. D. Meade, C. Clarke, F. Draux, G. D. Sockalingum, M. Manfait, F. M. Lyng and H. J. Byrne, *Anal. Bioanal. Chem.*, 2010, **396**, 1781–1791.
24 C. Krafft, T. Knetschke, R. H. W. Funk and R. Salzer, *Vib. Spectrosc.*, 2005, **38**, 85–93.
25 F. Draux, C. Gobinet, J. Sule-Suso, A. Trussardi, M. Manfait, P. Jeannesson and G. D. Sockalingum, *Anal. Bioanal. Chem.*, 2010, **397**, 2727–2737.
26 H. Nawaz, A. Garcia, A. D. Meade, F. M. Lyng and H. J. Byrne, *Analyst*, 2013, **138**, 6177–6184.
27 T. Wojcik, E. Buczek, K. Majzner, A. Kolodziejczyk, J. Miszczyk, P. Kaczara, W. Kwiatek, M. Baranska, M. Szymonski and S. Chlopicki, *Toxicol. in Vitro*, 2015, **29**, 512–521.
28 S. F. El-Mashtoly, D. Petersen, H. K. Yosef, A. Mosig, A. Reinacher-Schick, C. Kotting and K. Gerwert, *Analyst*, 2014, **139**, 1155–1161.
29 A. V. Feofanov, A. I. Grichine, L. A. Shitova, T. A. Karmakova, R. I. Yakubovskaya, M. Egret-Charlier and P. Vigny, *Biophys. J.*, 2000, **78**, 499–512.
30 Z. Farhane, F. Bonnier, A. Casey and H. J. Byrne, *Analyst*, 2015, **140**, 4212–4223.
31 K. Bräutigam, T. Bocklitz, A. Silge, C. Dierker, R. Ossig, J. Schnekenburger, D. Cialla, P. Rösch and J. Popp, *J. Mol. Struct.*, 2014, **1073**, 44–50.
32 L. Ahlinder, B. Ekstrand-Hammarström, P. Geladi and L. Österlund, *Biophys. J.*, 2013, **105**, 310–319.
33 K. Klein, A. M. Gigler, T. Aschenbrenner, R. Monetti, W. Bunk, F. Jamitzky, G. Morfill, R. W. Stark and J. Schlegel, *Biophys. J.*, 2012, **102**, 360–368.
34 A. Casey, E. Herzog, F. M. Lyng, H. J. Byrne, G. Chambers and M. Davoren, *Toxicol. Lett.*, 2008, **179**, 78–84.
35 P. Knief, C. Clarke, E. Herzog, M. Davoren, F. M. Lyng, A. D. Meade and H. J. Byrne, *Analyst*, 2009, **134**, 1182–1191.
36 M. S. P. Boyles, L. Young, D. M. Brown, L. MacCalman, H. Cowie, A. Moisala, F. Smail, P. J. W. Smith, L. Proudfoot, A. H. Windle and V. Stone, *Toxicol. in Vitro*, 2015, **29**, 1513–1528.
37 S. Wadhwa, C. Rea, P. O'Hare, A. Mathur, S. S. Roy, P. S. M. Dunlop, J. A. Byrne, G. Burke, B. Meenan and J. A. McLaughlin, *J. Hazard. Mater.*, 2011, **191**, 56–61.
38 F. Bonnier and H. J. Byrne, *Analyst*, 2012, **137**, 322–332.
39 P. Crow, B. Barrass, C. Kendall, M. Hart-Prieto, M. Wright, R. Persad and N. Stone, *Br. J. Cancer*, 2005, **92**, 2166–2170.
40 J. K. Pijanka, N. Stone, A. V. Rutter, N. Forsyth, G. D. Sockalingum, Y. Yang and J. Sule-Suso, *Analyst*, 2013, **138**, 5052–5058.
41 C. M. Krishna, G. D. Sockalingum, G. Kegelaer, S. Rubin, V. B. Kartha and M. Manfait, *Vib. Spectrosc.*, 2005, **38**, 95–100.
42 J. Riedl, S. Esslinger, C. Fauhl-Hassek and K. Kong, *Anal. Chim. Acta*, 2015, DOI: 10.1016/j.aca.2015.06.003.
43 B. A. Gutman, X. Hua, P. Rajagopalan, Y.-Y. Chou, Y. Wang, I. Yanovsky, A. W. Toga, C. R. Jack Jr., M. W. Weiner and P. M. Thompson, *NeuroImage*, 2013, **70**, 386–401.
44 Y. Oshima, H. Shinzawa, T. Takenaka, C. Furihata and H. Sato, *J. Biomed. Opt.*, 2010, **15**, 017009.
45 X. Zhang, H. Yin, J. M. Cooper and S. J. Haswell, *Anal. Bioanal. Chem.*, 2008, **390**, 833–840.
46 A. J. Hobro, M. Rouhi, E. W. Blanch and G. L. Conn, *Nucleic Acids Res.*, 2007, **35**, 1169–1177.
47 I. Notingher, *Sensors*, 2007, **7**, 1343–1358.
48 Y. Chen, Y. Su, L. Ou, L. Zou and Z. Chen, *Vibrational Spectroscopy*, 2015, DOI: 10.1016/j.vibspec.2015.06.004, Accepted manuscript 2 July 2015.
49 T. Tolstik, C. Marquardt, C. Matthaus, N. Bergner, C. Bielecki, C. Krafft, A. Stallmach and J. Popp, *Analyst*, 2014, **139**, 6036–6043.
50 O. C. Marina, C. K. Sanders and J. R. Mourant, *Biomed. Opt. Express*, 2012, **3**, 296–312.
51 R. Visintin and A. Amon, *Curr. Opin. Cell Biol.*, 2000, **12**, 372–377.
52 M. A. Jarboui, K. Wynne, G. Elia, W. W. Hall and V. W. Gautier, *Mol. Immunol.*, 2011, **49**, 441–452.
53 M. O. Olson, M. Dundr and A. Szebeni, *Trends Cell Biol.*, 2000, **10**, 189–196.
54 A. M. Hinsby, L. Kiemer, E. O. Karlberg, K. Lage, A. Fausbøll, A. S. Juncker, J. S. Andersen, M. Mann and S. Brunak, *Mol. Cell*, 2006, **22**, 285–295.
55 H. G. Schulze, S. O. Konorov, J. M. Piret, M. W. Blades and R. F. Turner, *Analyst*, 2013, **138**, 3416–3423.
56 A. N. Kuzmin, A. Pliss and A. V. Kachynski, *J. Raman Spectrosc.*, 2013, **44**, 198–204.